Linear Collider Collaboration Tech Notes

Study of Beam Energy Spectrum Measurement in the NLC Extraction Line

August 2000

Yuri Nosochkov and Tor Raubenheimer
Stanford Linear Accelerator Center
Stanford, CA

Abstract: The NLC extraction line optics includes a secondary focal point with a very small _-function and 2 cm dispersion which can be used for measurement of outgoing beam energy spread. In this study, we performed tracking simulations to transport the NLC disrupted beam from the Interaction Point (IP) to the extraction line secondary focus (the IP image), `measure' the transverse beam pro_le at the IP image and reconstruct the beam energy spectrum. The resultant distribution was compared with the original energy spectrum at the IP.

Study of Beam Energy Spectrum Measurement in the NLC Extraction Line*

Yuri Nosochkov and Tor Raubenheimer
Stanford Linear Accelerator Center, Stanford University, Stanford, CA 94309

Abstract

The NLC extraction line optics includes a secondary focal point with a very small β-function and 2 *cm* dispersion which can be used for measurement of outgoing beam energy spread. In this study, we performed tracking simulations to transport the NLC disrupted beam from the Interaction Point (IP) to the extraction line secondary focus (the IP image), 'measure' the transverse beam profile at the IP image and reconstruct the beam energy spectrum. The resultant distribution was compared with the original energy spectrum at the IP.

1 Introduction

The latest design of the NLC extraction line optics [1, 2] is shown in Fig. 1, where the outgoing beam travels from the IP (on the left) to the beam dump. The optics contains two groups of quadrupoles, where the first group performs a point-to-point focusing from the IP to the secondary focus, and the second group generates a parallel beam at the dump. The two quadrupole sets are separated by a symmetric chicane composed of four bends which generate 2 *cm* displacement and dispersion at the secondary focus. The original optics was designed with the horizontal chicane, but the vertical bends may be used as suggested by K. Kubo of KEK [3].

The purpose of the secondary focus with non-zero dispersion is to provide optimum conditions for measurement of the outgoing beam energy spread as well as for measurement with Compton polarimeter. For better energy resolution in the energy spectrum measurement, the beam dispersion $\eta\delta$ has to be large enough compared to the same plane energy dependent betatron beam size $\sigma = \sqrt{\beta(\delta)\epsilon}$ at the focus, where η is the linear dispersion, $\delta = \frac{\Delta p}{p}$ the relative momentum error, and ϵ the beam emittance.

The point-to-point transformation between the IP and the secondary focus is achieved with $R_{12} = R_{34} = 0$ and 180° phase advance, where R_{ij} are the linear matrix terms. According to this transformation and neglecting small coupling from detector solenoid, the on-momentum lattice functions at the secondary focus can be calculated as follows:

$$\beta_x = R_{11}^2\beta_x^*, \quad \beta_y = R_{33}^2\beta_y^*, \quad \alpha_x = \alpha_x^* - R_{11}R_{21}\beta_x^*, \quad \alpha_y = \alpha_y^* - R_{33}R_{43}\beta_y^*, \tag{1}$$

where $*$ denotes values at the IP, and the R-matrix terms for the present optics are

$$R_{11} = -4.5233, \quad R_{21} = -0.1019, \quad R_{33} = -0.4549, \quad R_{43} = -0.1299. \tag{2}$$

Note that point-to-point transformation and comparable distance from IP and secondary focus to the quadrupoles between them automatically result in low β-functions at the secondary focus.

Several scenarios for the NLC beam parameters are presently under consideration [4]. In this study, we used one particular set of parameters called 'NLC 1 TeV Case A'. Some of the parameters

*Work supported by Department of Energy contract DE–AC03–76SF00515.

for this case are shown in Table 1. The 'disrupted' and 'undisrupted' parameters stand for beams with and without collision, respectively. For the NLC design the beam-beam interaction forces are large enough to distort ('disrupt') the incoming beam phase space at IP. Notably, the beam divergence, emittance and energy spread are significantly increased in the collision for 0.5 TeV beams. The particle phase space distribution at the IP after collision was obtained using GUINEA–PIG code [5, 6], and the corresponding disrupted emittance and lattice functions were reconstructed from this distribution. The disrupted β^* and α^* have to be used in Eq. 1.

Table 1: IP beam parameters (NLC 1 TeV case A).

Beam parameter	Undisrupted x/y	Disrupted x/y
Emittance (m·rad) $[10^{-13}]$	39/0.59	120/1.02
rms beam size (nm)	198/2.7	198/3.2
rms divergence (μrad)	20/22	125/33
β^* (mm)	10/0.125	3.259/0.103
α^*	0/0	1.805/0.306
Energy cms (GeV)	1046	
Particles per bunch	$0.75 \cdot 10^{10}$	
Bunches per train	95	
Repetition rate (Hz)	120	
Disruption parameter	0.094/6.9	
Average energy loss per particle	9.5%	

According to Table 1 and Eqs. 1 and 2, the optics with vertical chicane should provide more accurate measurement of the beam energy spectrum because the vertical betatron size $\sqrt{\beta_y \epsilon_y}$ at the secondary focus is smaller than in the horizontal plane, while the dispersion is the same. Note, however, that $\beta_{x,y}$ at the focus can grow significantly as a function of energy due to longitudinal displacement of the $\beta(\delta)$ waist.

Below we describe simulations of the beam energy spectrum measurement for two options of the extraction line: with 1) horizontal and 2) vertical chicane, and $\eta = 2$ *cm* dispersion. Based on this study, we will examine the energy resolution in this measurement and select the preferred orientation of the chicane. We should also note that the optics with vertical chicane used in this study is a duplicate of the horizontal optics, except the bends were set to the vertical plane. A small difference in the vertical bend edge focusing was not corrected and may have slightly distorted the β-value at the secondary focus, however it is insignificant compared to energy dependent effects. The effect of corrected 6 T detector solenoid was included in the simulations.

2 Simulations

Using GUINEA–PIG code [5, 6], the disrupted distribution of 50,000 particles was generated at the IP. It has a very wide energy spread which is shown in Fig. 2. This distribution was tracked from the IP to the secondary focus using the NLC version of DIMAD code which correctly accounts for large energy errors [7].

The non-zero dispersion and small betatron size at the secondary focus result in significant

correlation between a particle transverse position and energy. This makes it possible to reconstruct the beam energy spectrum based on beam profile measurement at the secondary focus, such as wire scanner measurement.

Correlation between particle position and energy at the secondary focus comes from energy dependent deflection in the chicane. Neglecting small edge focusing in the bends, one can find that a particle coming on axis into chicane will have a transverse deflection

$$x_\eta = \frac{\eta\delta}{1+\delta} \tag{3}$$

at the secondary focus, where x_η is a horizontal or vertical deflection with respect to the on-energy reference orbit. Eq. 3 can be used to estimate the particle energy deviation δ based on measured x or y-deflections and known η at the secondary focus:

$$\delta = \frac{x}{\eta - x}. \tag{4}$$

Using Eq. 4, one can also convert measured beam profile $N(x)$ into beam energy spectrum $N(\delta)$.

Eq. 4 is only correct if deflections x and y are caused entirely by dispersion and particle δ is constant. In reality, several other factors contribute to particle deflection at the secondary focus:

- Betatron motion $\sim \sqrt{\beta(\delta)\epsilon}$ smears particles around their energy dependent reference orbit x_η.
- Synchrotron radiation causes random loss of particle energy which changes particle deflections in the magnets. According to DIMAD simulations with 0.5 TeV beam, an average change in δ between the IP and secondary focus is -0.0015. The effect on particle position at the secondary focus depends where the energy loss has occurred and, relatively, has more impact on particles with small δ.
- Quadrupole misalignment and bending field errors generate additional energy dependent deflections.
- Beam offset x^*, y^* at the IP causes systematic offset at the secondary focus: $R_{11}(\delta)x^*$, $R_{33}(\delta)y^*$.

Measurement errors have to be taken into account as well.

Denoting the above contributions as Δx, particle deflection at the secondary focus can be expressed as $x = x_\eta + \Delta x$. Clearly, the accuracy of Eq. 4 improves if Δx is small compared to x_η. This particularly requires that the beam betatron size $\sqrt{\beta(\delta)\epsilon}$ at the secondary focus is small compared to x_η.

2.1 Energy Resolution Analysis

To be able to reconstruct the beam energy spectrum based on beam profile measurement, particles with different energies have to be well separated in space in a systematic way. To verify the actual dependence of particle positions on energy, we generated and analyzed beam distribution at the secondary focus. Disrupted beam with 50,000 particles was tracked from the IP to the secondary focus using DIMAD code. The simulation included synchrotron radiation effects, but no magnet errors were applied.

Fig. 3 shows distribution of particle positions vs. δ at the secondary focus for horizontal and vertical chicane, respectively. The solid line is the analytic displacement due to dispersion: x_η or

y_η in Eq. 3. Since we want to reconstruct the initial energy spectrum at the IP, the distributions in Fig. 3 are plotted against initial particle δ at IP. Note that the particle energy at the secondary focus is slightly reduced by the amount of synchrotron radiation energy loss after IP.

Fig. 3 shows that in the horizontal case the larger betatron size makes a wider particle spread around x_η compared to the spread in the vertical case. In the beam profile measurement, the number of particles is counted per x or y-slices across the beam. With the horizontal chicane, each x-slice contains particles with rather wide range of energies which would make energy analysis more difficult. In the vertical case, the particle deflections are dominated by the dispersion which should improve accuracy of the energy estimate with Eq. 4.

The energy resolution based on beam profile measurement can be further examined by dividing the simulated beam into slices with different energies and evaluating spatial separation between them. For each monochromatic slice, we collected all particles with the corresponding energy and then calculated its *rms* size and (x,y)-position and orientation. Fig. 4 and 5 show these slices in the form of one sigma beam ellipses for different energies on the x-y plane. Clearly, the vertical chicane optics provides greater separation between different slices and, therefore, should result in better energy resolution.

The ellipses in Fig. 4 and 5 are plotted against initial particle δ at the IP. Synchrotron radiation between the IP and the secondary focus reduces δ by an average amount of 0.0015 which slightly distorts particle deflections. This mostly affects particles with small δ. One can see for instance that ellipses at $\delta = 0$ in Fig. 4 and 5 are disproportionally wide in the direction of dispersion. This is because the initially on-energy particles experience energy loss after IP which increases deflections due to dispersion in bends and stronger focusing. This effect is negligible for particles with $|\,\delta\,| > 1\%$.

The beam size of the above energy slices at the secondary focus can be plotted against δ as shown in Fig. 6. Within the energy range on the plot, the beam size is approximately proportional to $|\,\delta\,|$, which can be interpreted as $\beta \sim \delta^2$. This dependence can be explained by analyzing the formula for energy dependent β-function at the secondary focus:

$$\beta_x(\delta) = R_{11}^2(\delta)\beta_x^* - 2R_{11}(\delta)R_{12}(\delta)\alpha_x^* + R_{12}^2(\delta)\frac{1+\alpha_x^{*2}}{\beta_x^*}, \tag{5}$$

and similar for $\beta_y(\delta)$. For point-to-point transformation, the R_{11} and R_{12} terms as a function of δ can be written as

$$R_{11}(\delta) = R_{11}(0) + O(\delta) + high\ order\ terms, \tag{6}$$

$$R_{12}(\delta) = O(\delta) + high\ order\ terms. \tag{7}$$

According to Eqs. 6 and 7, the first two terms in Eq. 5 may have non-zero linear terms in δ, but the lowest order in the third term is quadratic. Due to the very small value of β^*, the third term is significantly amplified by $1/\beta^*$ factor and becomes dominant, except for very small $|\,\delta\,|$. Since the $R_{12}(\delta)$ term is proportional to phase shift at the secondary focus, one can conclude that quadratic growth of $\beta(\delta)$ comes mostly from the β-waist shift. Another analysis of the $\beta(\delta)$ dependence can be done using a simplified model consisting of a drift after IP, a focusing quadrupole and another drift before the secondary focus. In this model, the $R(\delta)$-terms can be easily derived, and numerical estimate showed that δ^2-term in $\beta(\delta)$ is dominant at $|\,\delta\,| > 0.1\%$. At very low energy higher order chromatic effects may be important.

Based on ellipses in Fig. 4 and 5, a ratio of average particle displacement at the secondary focus to beam size as a function of δ is plotted in Fig. 7. Due to smaller beam size, the optics with

vertical chicane has this ratio almost a factor of 3 larger compared to the horizontal optics and, therefore, is better for energy resolution. At δ near zero, the vertical ratio is somewhat reduced due to the effect of synchrotron radiation energy loss. When δ approaches to -1, the average particle displacement increases hyperbolically as $\eta\delta/(1+\delta)$ which may improve energy separation at the low energy end.

2.2 Simulation of Energy Spectrum Measurement

Simulation of the beam energy spectrum measurement included the following steps.

Beam Profile Measurement

First, we simulated the beam profile measurement at the secondary focus. The beam distribution was obtained by tracking 50,000 particles from the IP as described earlier. In the study, we assumed that the beam profile measurement is done in 50 μm steps over the range of 25 mm in the direction of dispersion at the secondary focus. In each step, the number of particles was counted within the corresponding 50 μm x or y-bins for horizontal and vertical chicane, respectively. As a result, a histogram $N(x)$ or $N(y)$ was obtained for the beam profile, where N is the number of particles per bin. The particles beyond the range of 25 mm were not included in the measurement due to rather low statistics in the simulation. Measurement errors were not taken into account in this calculation.

Reconstruction of Energy Spectrum

To estimate beam energy spectrum $N(\delta)$ from the obtained horizontal $N(x)$ or vertical $N(y)$ beam profile, we used Eq. 4 to convert x or y-bins into δ-bins. According to Eq. 4, the width of δ-bin varies with x as

$$\Delta_\delta = \frac{\eta}{(\eta - x)^2}\Delta_x, \tag{8}$$

where Δ_x is the bin-width in x or y-plane. For $\Delta_x = \Delta_y = 50$ μm and 2 cm dispersion, the δ bin-width gradually reduces from 0.25% at $x = y = 0$ to 0.05% at -25 mm. To avoid dependence of $N(\delta)$ on Δ_δ, we normalized it to the corresponding bin-width. For a more general result, we also normalized $N(\delta)$ to the total number of particles N_{tot} in the histogram. The resultant energy distribution $dN/d\delta/N_{tot}$ was compared with the initial spectrum at the IP. Both histograms are shown in Fig. 8 for the horizontal and vertical chicane, where the blue line (darker shade) is for the initial spectrum at the IP and the green line for the 'measured' spectrum. The energy range in Fig. 8 ends at about $\delta = -55\%$ due to 25 mm range used in the beam profile measurement.

Clearly, optics with the vertical chicane provides more accurate measurement of energy spectrum. In the horizontal case, the reconstructed spectrum shows more particles in the $\delta > 0$ range than are present in the original distribution. This is due to relatively large horizontal beam size. It results in some particles having positive betatron x-deflections which are interpreted as positive δ in Eq. 4. Note that logarithmic scale in Fig. 8 somewhat exaggerates the size of the $\delta > 0$ tail.

More detailed view of the above distributions at small δ is shown in Fig. 9. One can see that the measured spectrum in the vertical case even reproduces the incoming beam double horned energy profile near $\delta = 0$, while the histogram with horizontal chicane is not accurate in this range.

Ratio of the measured to original spectrum $N_{meas}(\delta)/N_{IP}(\delta)$ is shown in Fig. 10. It confirms that the spectrum obtained with vertical chicane is a closer match to the original distribution.

The most uncertainty in the measurement appears at $\delta \geq 0$ and at the very low energy end. The measurement error at $\delta \geq 0$ is the result of positive betatron deflections exceeding dispersion related deflections. Energy loss due to synchrotron radiation also contributes to distortion near $\delta = 0$. At the very low energies, the accuracy is reduced due to low particle statistics in the simulated beam and smaller bin-width Δ_δ. According to Eq. 8, to keep Δ_δ constant one would need to obtain the beam profile $N(x)$ with bin-width Δ_x increasing quadratically with x:

$$\Delta_x = \frac{(\eta - x)^2}{\eta} \Delta_\delta. \tag{9}$$

3 Conclusion

Analysis of the beam energy spectrum based on beam profile measurement at the secondary focus in the NLC extraction line showed that the reconstructed energy profile reasonably matches the original distribution at IP. The optics with vertical chicane is preferred because it provides better energy resolution due to smaller ratio of betatron size to dispersion at the secondary focus compared to the horizontal case. Effects of beam, magnet and measurement errors on the energy spectrum measurement need to be evaluated in future studies.

References

[1] Y. Nosochkov, *et al.*, "*The Next Linear Collider Extraction Line Design*," Proceedings of the 1999 IEEE Part. Acc. Conf. (PAC99), New York City, NY (1999); SLAC–PUB–8096 (1999).

[2] Y.M. Nosochkov and T.O. Raubenheimer, "*NLC Extraction Line Studies*," SLAC–PUB–8313 (1999).

[3] K. Kubo, presented at ISG5 Workshop (2000).

[4] K.A. Thompson and T.O. Raubenheimer, "*Luminosity for NLC Design Variations*," SLAC note LCC–0014 (1999).

[5] D. Schulte, TESLA–97–08 (1996).

[6] K.A. Thompson provided the disrupted beam distribution at IP, generated with GUINEA–PIG code.

[7] P. Tenenbaum, *et al.*, "*Use of Simulation Programs for the Modeling of the Next Linear Collider*," SLAC–PUB–8136 (1999).

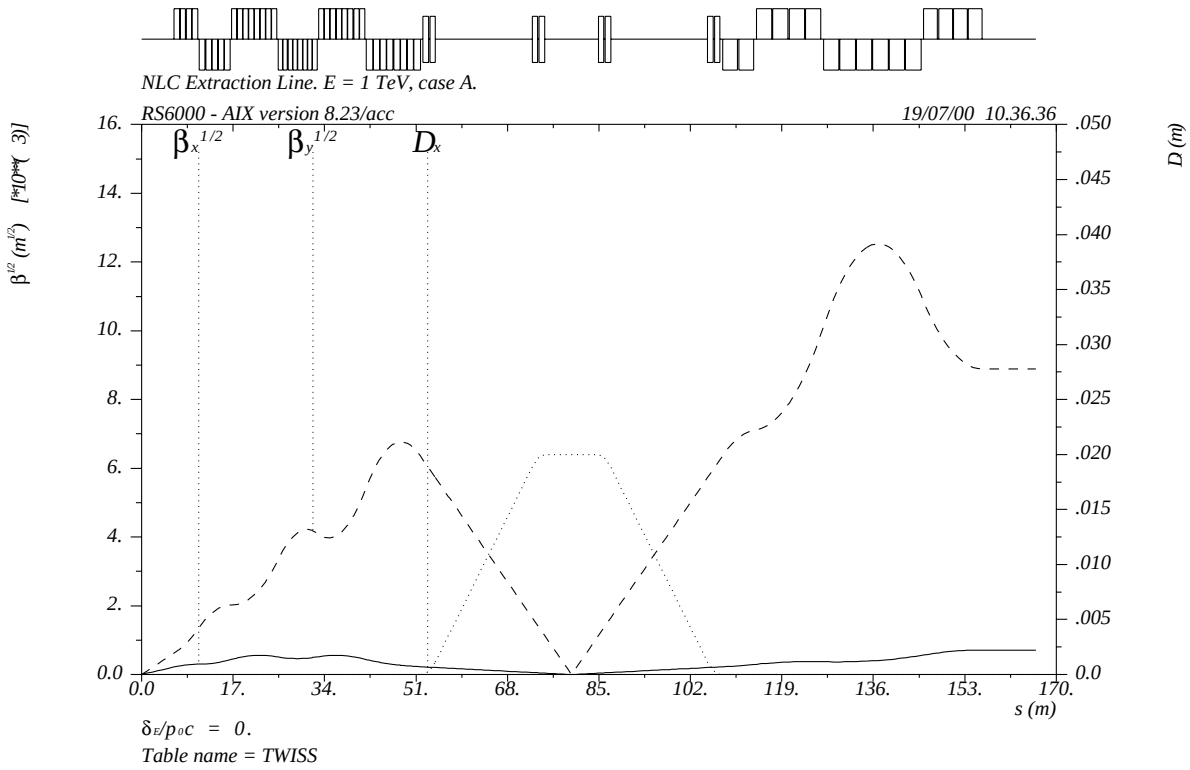

Figure 1: Lattice functions in the NLC extraction line for '1 TeV case A' beam parameters (IP is on the left).

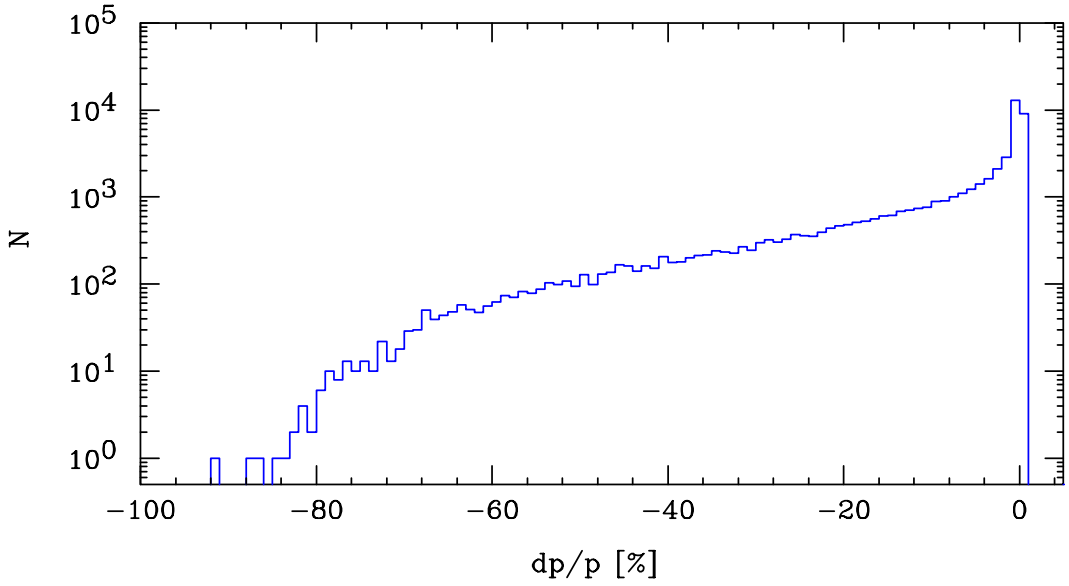

Figure 2: Disrupted beam energy spread at the IP for 50,000 particles (NLC 1 TeV case A).

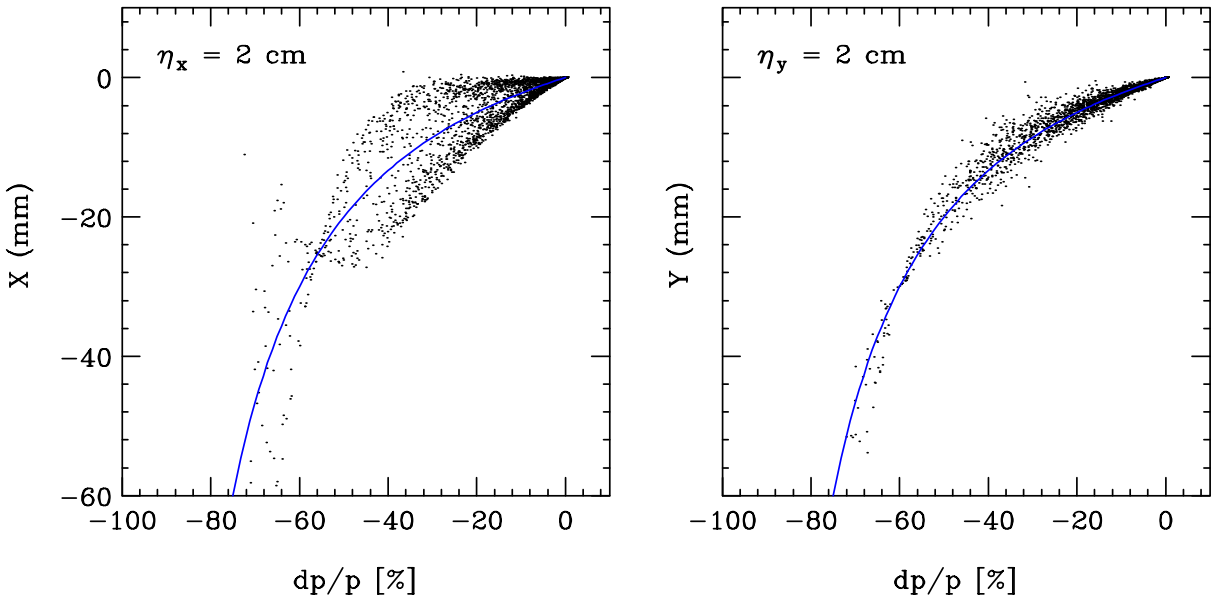

Figure 3: Horizontal and vertical distribution vs. δ at the secondary focus for horizontal and vertical chicane, respectively. Solid line shows deflection due to dispersion $\eta\delta/(1+\delta)$.

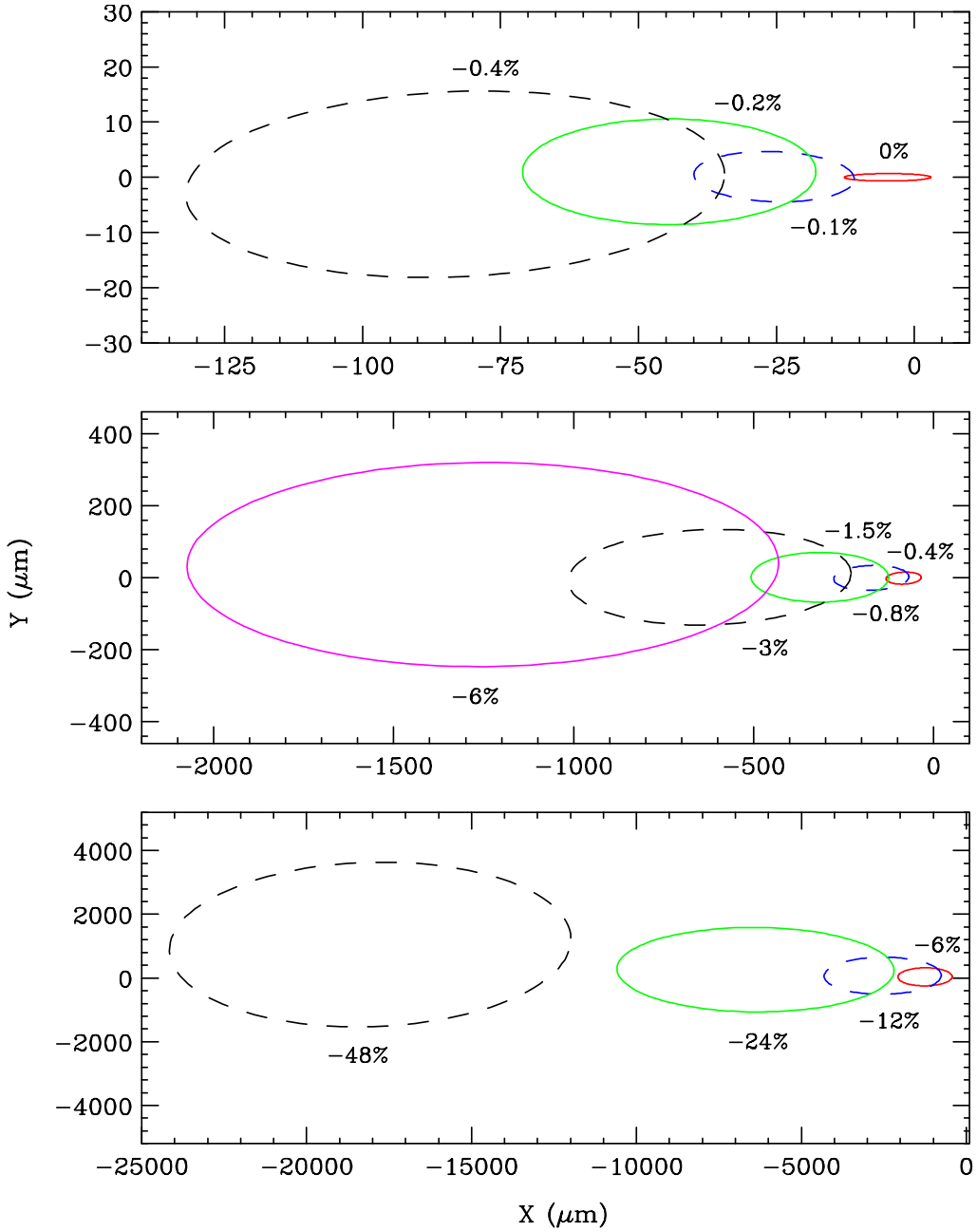

Figure 4: One sigma beam ellipses for particles with different δ at the secondary focus with horizontal chicane.

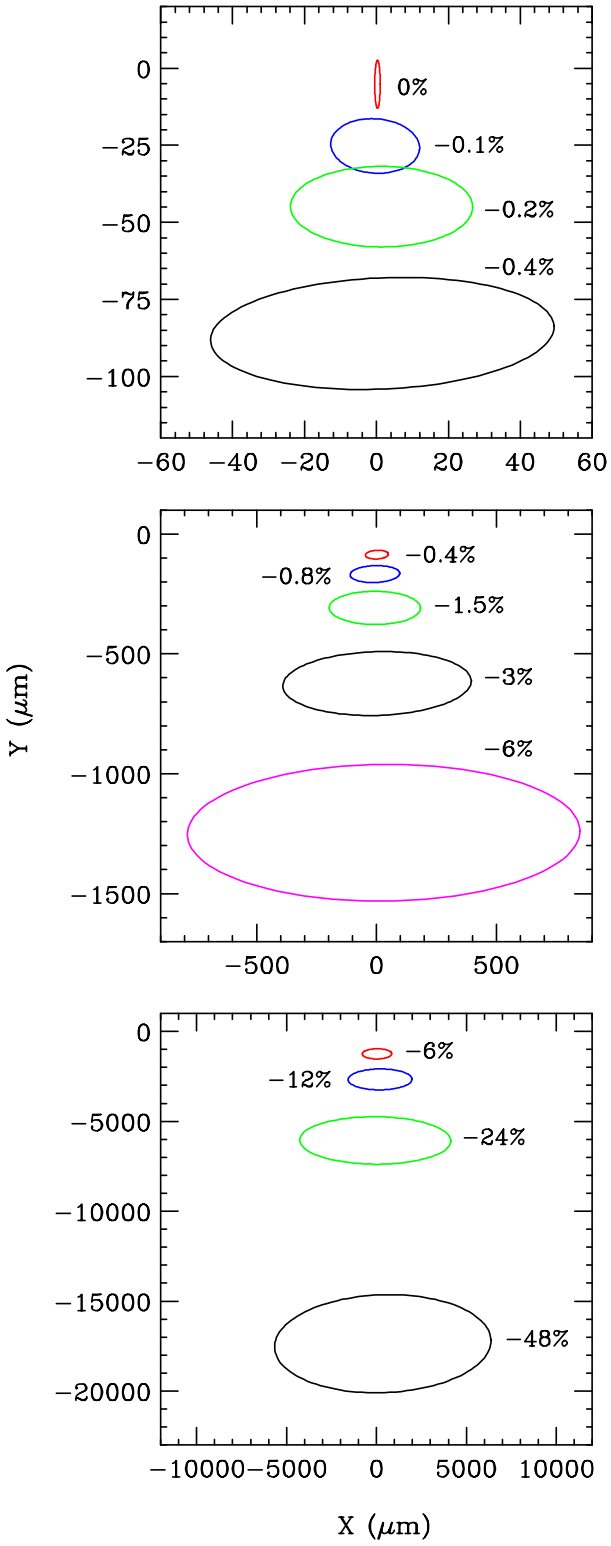

Figure 5: One sigma beam ellipses for particles with different δ at the secondary focus with vertical chicane.

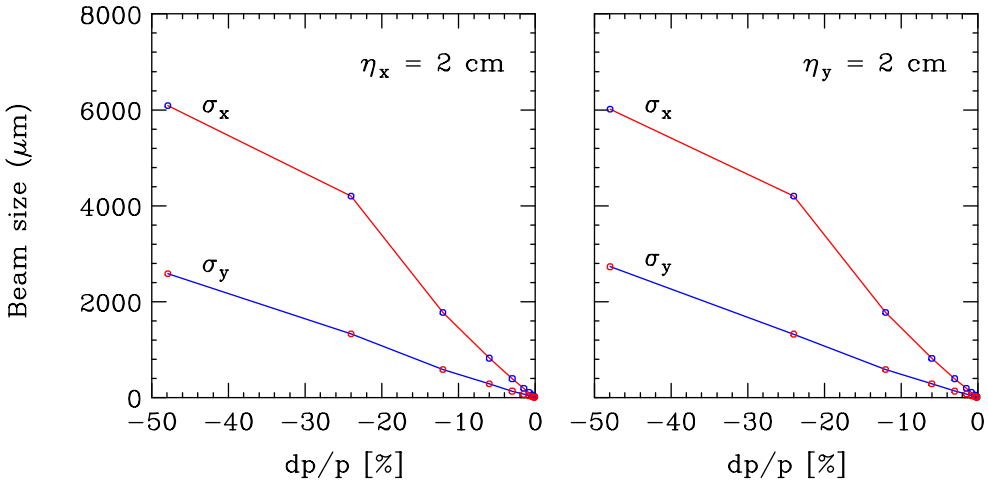

Figure 6: One sigma beam size at the secondary focus vs. δ for optics with horizontal and vertical chicane.

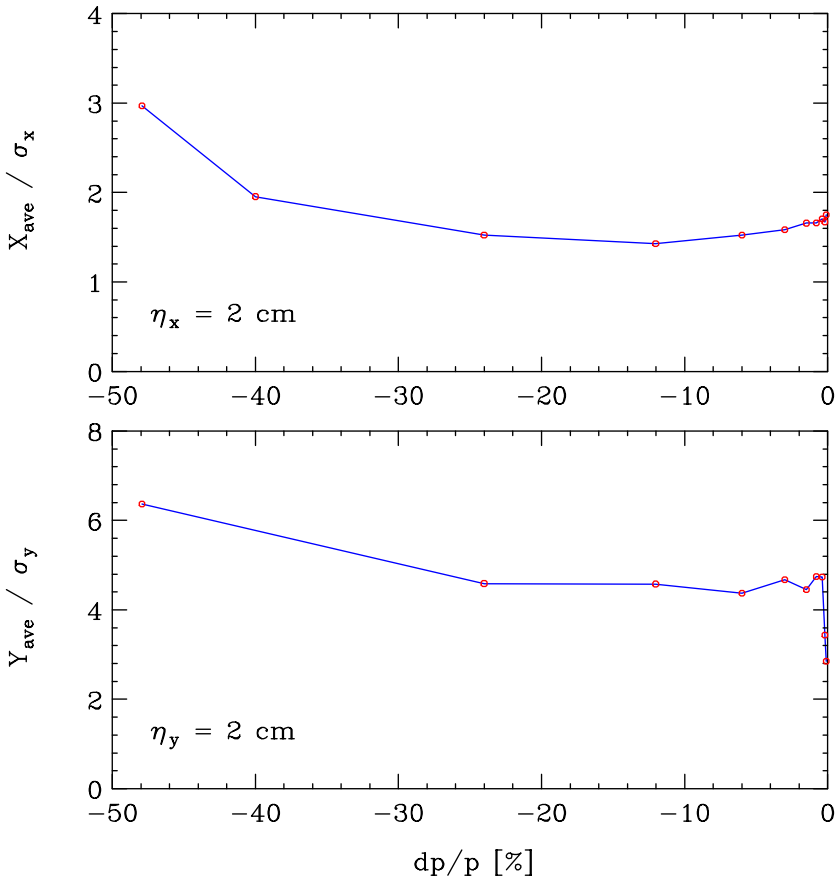

Figure 7: Ratio of average particle displacement to *rms* beam size at the secondary focus vs. δ for optics with horizontal and vertical chicane.

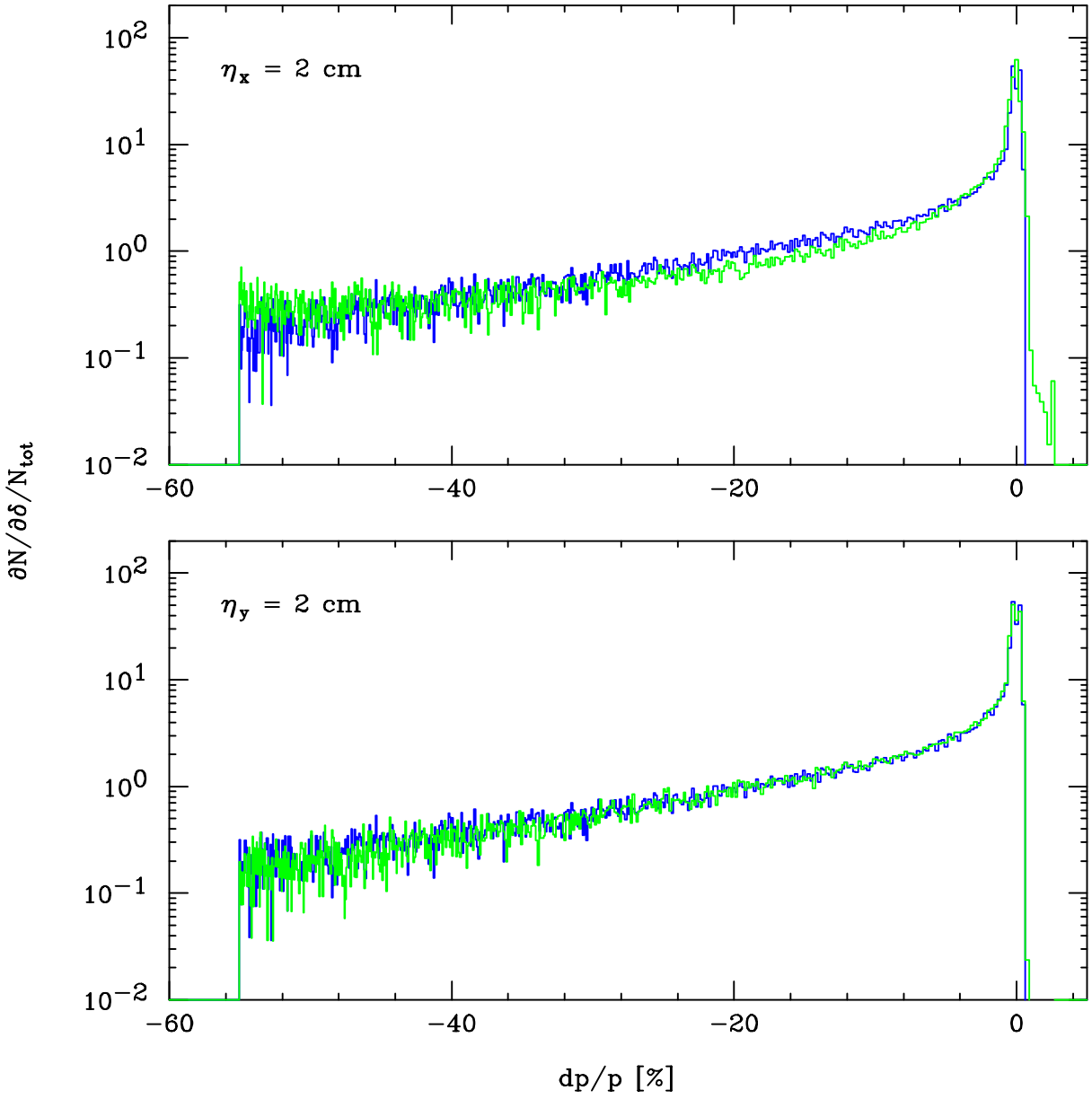

Figure 8: Original (blue, darker shade) and measured (green) energy spectrum $dN/d\delta/N_{tot}$ for horizontal and vertical chicane.

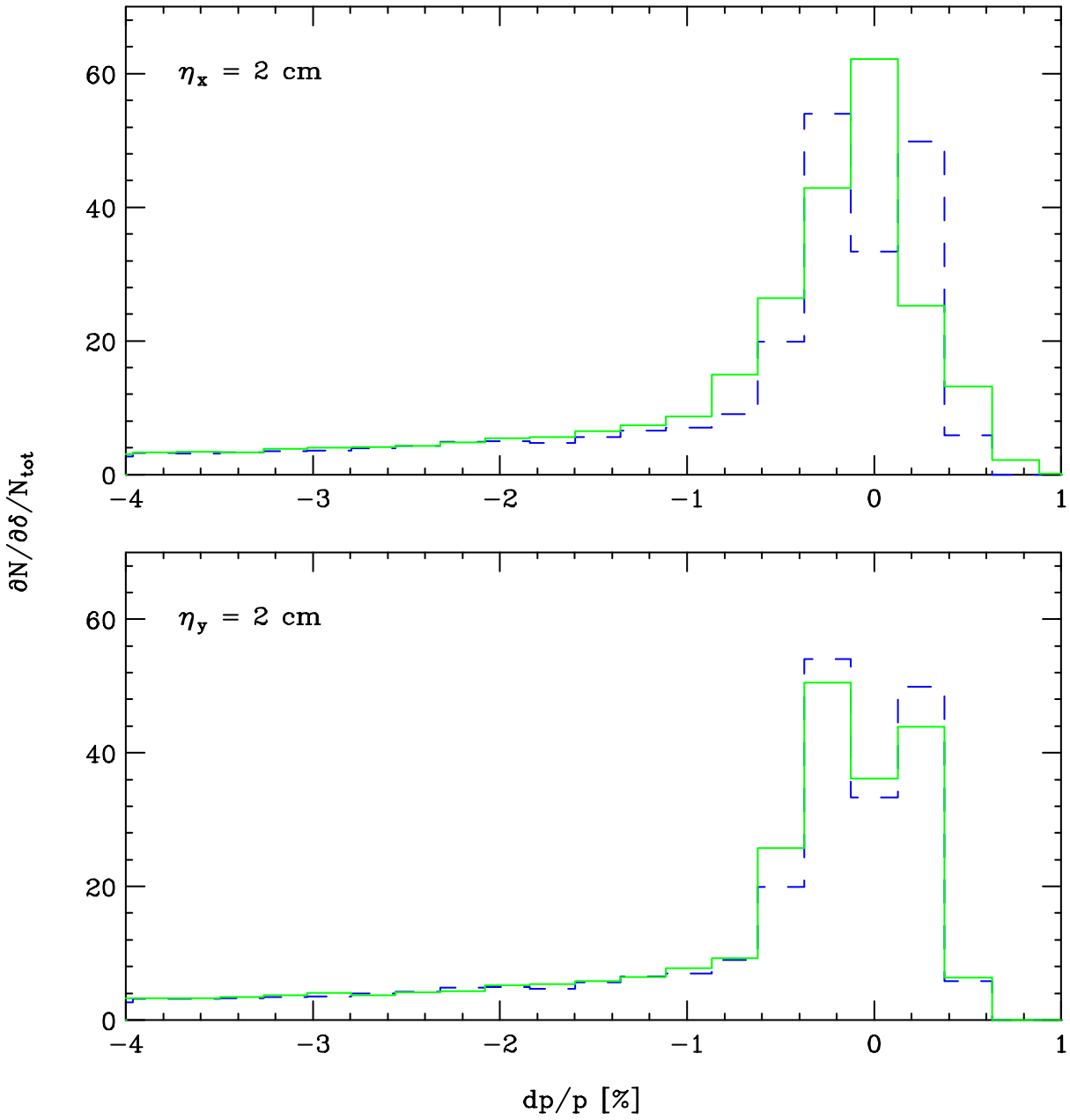

Figure 9: Original (blue dash) and measured (green) energy spectrum $dN/d\delta/N_{tot}$ near $\delta = 0$ for horizontal and vertical chicane.

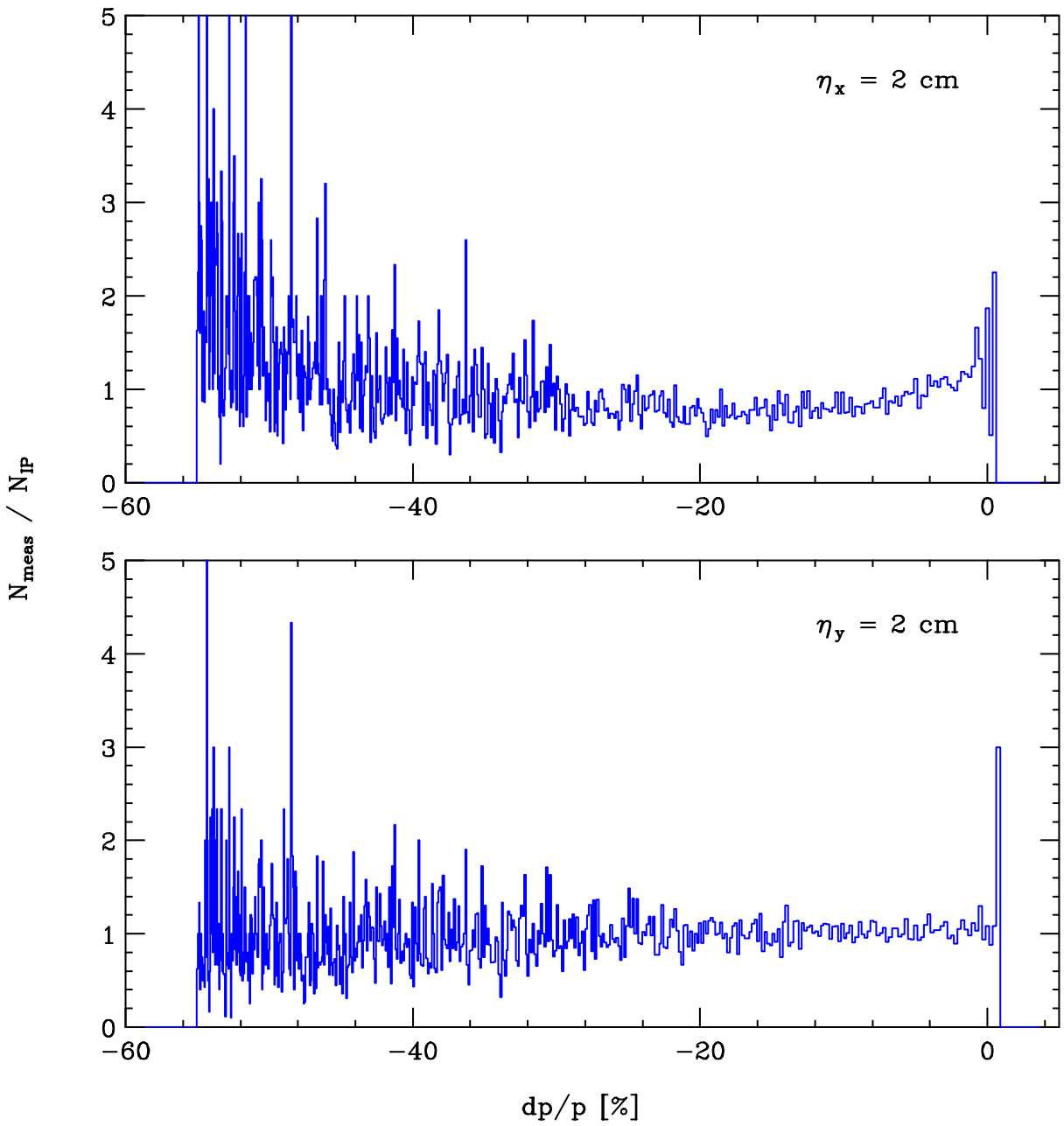

Figure 10: Ratio of measured to the original energy spectrum $N_{meas}(\delta)/N_{IP}(\delta)$ for horizontal and vertical chicane.